PHYSICAL REVIEW B **84**, 235443 (2011)

Interplay between interfacial and structural properties on the magnetism of self-organized core-shell Co/Pt supported nanodots

P. Campiglio,[*] N. Moreau, V. Repain,[†] C. Chacon, Y. Girard, J. Klein, J. Lagoute, and S. Rousset
Laboratoire Matériaux et Phénomènes Quantiques, Université Paris Diderot Paris 7, Sorbonne Paris Cité, Centre National de la Recherche Scientifique, Joint Research Units 7162 Case Courrier 7021, FR-75205 Paris 13, France

H. Bulou, F. Scheurer, and C. Goyhenex
Institut de Physique et Chimie des Matériaux de Strasbourg, Université Louis Pasteur and Centre National de la Recherche Scientifique, Joint Research Units 7504, Boîte Postale 43, FR-67034 Strasbourg, France

P. Ohresser and E. Fonda
Synchrotron SOLEIL, L'Orme des Merisiers, Saint-Aubin, BP 48, FR-91192 Gif sur Yvette, France

H. Magnan
Service de Physique et de Chimie des Surfaces et des Interfaces, IRAMIS, Commissariat a l'Energie Atomique Saclay, FR-91191 Gif sur Yvette, France

(Received 25 October 2011; revised manuscript received 6 December 2011; published 27 December 2011)

We have studied the influence of Pt capping on the magnetic properties of self-organized Co nanodots by means of complementary structural and magnetic investigation techniques. The growth of monodisperse 5 nm diameter Co dots on a Au(111) surface and its progressive coverage by Pt were performed under ultrahigh vacuum conditions and imaged by scanning tunneling microscopy, revealing a weak mixing at room temperature. The Co/Pt core-shell structure was studied both by molecular-dynamics simulations and surface extended x-ray-absorption fine structure, showing a global dilatation of the Co core. Both magnetic moments and hysteresis cycles at various temperatures were measured using x-ray magnetic circular dichroism, revealing a slight increase of the magnetic moments and the out-of-plane magnetic anisotropy after Pt capping. Moreover, the variation of magnetic anisotropy as a function of capping was followed *in situ* by the magneto-optical Kerr effect. Our investigations demonstrate that interfacial hybridization between Co and Pt is dominant over magnetoelastic contribution in this system.

DOI: 10.1103/PhysRevB.84.235443 PACS number(s): 75.50.Tt

I. INTRODUCTION

Core-shell nanoparticles have received increasing attention in order to practically use magnetic clusters in applications and devices.[1,2] The growing interest around these systems is due to several reasons. First of all, the shell protects the magnetism of the core, which readily oxidizes in environmental conditions. Moreover, the shell can donate to the particle new chemicophysical functionalities which, combined with magnetism, result in multifunctional systems with possible applications from catalysis to biomedicine. From a more fundamental point of view, the capping of nanoparticles is a convenient and straightforward route to modify the magnetic (more generally, the physical) properties of the clusters, by exploiting the primary role of interfaces in low-dimensional systems. In particular, a key quantity that has to be controlled is the magnetic anisotropy energy (MAE), which governs the stability of the magnetization along the easy-axis direction. When magnetic nanoparticles are covered with a capping layer, several phenomena set in.[3] These include structural contributions such as strain, chemical intermixing, surface roughness, size and shape, as well as electronic contributions due to interfacial hybridization between the nanoparticles and the overlayer. All these contributions have to be disentangled to be able to tailor the MAE for specific applications.

This ability is particularly important in magnetic data storage, where it is necessary to enhance MAE in order to continuously increase the areal storage density in future memories. Self-organized supported nanodots are promising candidates to follow the current trend[4] since they can offer a recording density higher than 20 Tb/in.^{2}, but it remains necessary to improve the magnetic stability of such small nanostructures against thermal excitations.[5] The capping with a nonmagnetic metal can provide a convenient route to achieve this goal, following what has been demonstrated in the past in the case of ultrathin films. For such a purpose, Pt seems to be a good candidate. Indeed, Co nanostructures on Pt(111) display a strong out-of-plane magnetic anisotropy,[6] even further increased when reducing the cluster sizes down to the single atom.[7] Moreover, it is known that a Pt overlayer increases the out-of-plane anisotropy in Co ultrathin films,[8] which is even enhanced in Co/Pt multilayers.[9,10]

In this work we investigate the effect of Pt capping on the magnetic behavior of Co nanodots, in order to extend the study of its effect on zero-dimensional systems. In this case, the more pronounced symmetry breaking can lead to a different balance between mixing, strain, and electronic hybridization, generally resulting from metal capping. In particular, we used Co nanodots which are self-organized on Au(111).[11] This is a model system since the reconstruction of the Au surface guides the Co growth toward the formation of a well-ordered array of nanodots with tunable size up to a few nanometers. Moreover, since the islands are quasi-monodisperse, averaging measurements over a macroscopic area reflects single-dot properties, allowing us to unambiguously determine their properties.[12,13] Structural analysis was carried out by means of surface extended x-ray-absorption fine structure (SEXAFS) and molecular-dynamics calculations. The evolution of the Co magnetism with Pt capping was studied with x-ray magnetic circular dichroism (XMCD) and the magneto-optical Kerr effect (MOKE).

A. Experimental details

The samples used in this work were grown and characterized in several ultrahigh vacuum apparatus for *in situ* sample preparation and characterization, depending on the analysis techniques. In all cases, we used the same procedure for substrate cleaning and sample growth. The substrate is a Au(111) oriented single-crystal sample, displaying a mirrorlike surface and 300 nm wide terraces. Once introduced in the UHV apparatus (base pressure better than 1×10^{-10} mbar), it was cleaned with repeated cycles of bombardment with Ar ions ($p_{\mathrm{Ar}} = 2 \times 10^{-6}$ mbar, $V = 1$ kV) followed by annealing at 450 °C. Cobalt and platinum were evaporated by electron bombardment heating of high-purity rods (99.99%), while the substrate was kept at room temperature. Typical flux rates were 0.2 ML (monolayer)/min and 0.02 ML/min for Co and Pt, respectively. These were calibrated by the submonolayer deposition of Co or Pt and a flooding procedure of scanning tunneling microscope (STM) images. Then, the cobalt and platinum coverage (θ_{Co} and θ_{Pt}) were determined by the deposition time. Alternatively, for SEXAFS measurements, a quartz-crystal microbalance, and auger electron spectroscopy were used.

X-ray-absorption spectroscopy (XAS) data were recorded at the SAMBA beamline of the SOLEIL synchrotron radiation center (Gif-sur-Yvette, France)[14] on the SEXAFS setup. Harmonic rejection was obtained by using two Pd-coated Si mirrors, whereas the sagittaly focusing Si (220) monochromator was operated fully tuned. X rays were linearly polarized along the x axis, while the sample could be rotated around the z axis; we could, thus, modulate the sensitivity to in-plane and out-of-plane structures. Measurements were performed in fluorescence mode with a seven-element Ge solid-state detector observing the sample at 90 ° with respect to incoming x rays; the distance to the sample could be varied to keep the count rate in the linear regime without breaking the vacuum. Absence of contaminants in the Au crystal was checked by fluorescence detection with an excitation energy of 12 keV before Co and Pt evaporation and after cleaning of the substrate. The variation of the x-ray-absorption coefficient of samples was measured at 77 K above the K edge of cobalt (7709 eV). To get information about the anisotropy of the crystallographic structure, two spectra were recorded for each sample: one in normal incidence (NI) (polarization of the x ray parallel to the surface plane of the substrate) and one in grazing incidence (GI) where the polarization of the x rays was about 75 ° out of the surface plane.

The structural evolution of the Co dots during Pt encapsulation was simulated by using molecular-dynamics calculations. The forces involved in the process were derived from the total energy defined as the sum of the overall site energies. The site energies are based on effective potentials determined in the second-moment approximation of the tight-binding theory[15] with the constraints (i) to reproduce the main features of the phase diagrams for the mixed interactions and the cohesive energy, the lattice parameter, the bulk modulus, and the elastic constants for pure ones and (ii) to preserve the correct surface energy difference for each couple of pure metals.[16,17] The time integration was performed by using a velocities Verlet integration algorithm.[18,19] We used a large simulation slab containing 18 000 Au atoms, distributed on twelve (111) planes (50×30 Au atoms per plane), on top of which a nanocluster consisting of 585 Co adatoms was deposited, corresponding to an experimental deposit of 0.3 ML. Periodic boundary conditions were applied in the directions parallel to the substrate. Atomic positions of the initial cluster and the substrate atoms were determined by using a quench procedure. The encapsulation process was performed through successive cycles of Pt deposition also followed by a quench procedure to fully relax the geometry at each step. Each Pt adatom was deposited in contact with the cluster, and a layer-by-layer process was considered in agreement with experiments. Usually, in order to avoid local minima, a free temporal evolution on 10 ps at 300 K was performed before quenching.[20] However, in the present case, such a procedure lead to a strong interdiffusion between Co and Pt, even at temperature as low as 100 K, due to the order tendency of the Pt-Co system and the ternary feature of the interface between Co and Pt deposited on gold. In order to keep the Pt-Co interface as clean as possible, no free temporal evolution was considered, and the initial temperature of the quench process was set up from the excess of potential energy resulting from the initial position of the Pt adatom.

XMCD experiments were carried out at the beamline ID08 of the European Synchrotron Radiation Facility (Grenoble). The XMCD signal was obtained by the difference in the XAS signal at the Co $L_{2,3}$ edges recorded for left- and right-circularly polarized light taking the direction of the magnetic field as the quantization axis.[21] The station provided 100% circularly polarized lights and a 7 T magnetic field out of a superconducting magnet. The applied field was aligned with the photon propagation vector. By rotating the sample at an angle α it could be magnetized along different directions, allowing angle-resolved measurements. The minimum temperature on the sample was around 10 K. The magnetic susceptibility was measured by the magneto-optical Kerr effect with a 1-Hz AC field ($H_{\mathrm{rms}} = 10$ mT) generated by an *ex situ* coil and in the temperature range from 40 to 300 K. The optical signal was detected through a crossed-polarizers configuration. The real and imaginary parts of the dynamical susceptibility (χ' and χ'') were measured with a lock-in amplifier.

II. EXPERIMENTAL RESULTS

A. Growth of Co/Pt supported nanodots

During the first stage of growth, Co nucleates at the elbows of Au(111) herringbone reconstruction[22] through an exchange mechanism.[23] In the submonolayer regime, Co forms dots with

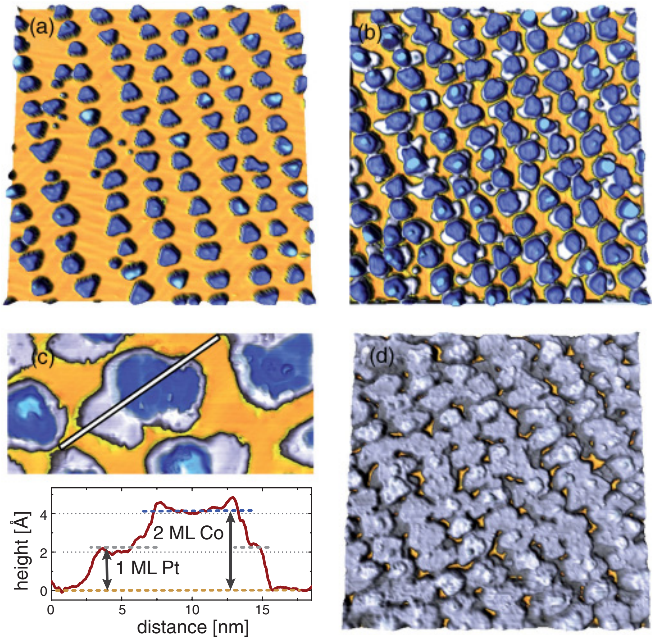

FIG. 1. (Color online) Three-dimensional views of STM images (100×100 nm^2) showing the growth of Pt around and on the top of Co nanoislands. The color scale is intended to represent the different elements of the system (yellow: Au; blue: Co; gray: Pt). (a) 0.5 ML of Co. (b) 0.5 ML of Pt surrounding Co islands. (c) STM image (30×15 nm^2) and profile analysis of a typical Pt-rim/Co-core dots. (d) 1.5 ML of Pt deposited on Co.

an apparent height of 4.1 Å, corresponding to the distance between two hcp Co(0001) planes.[11,24] The dots are well arranged in arrays driven by the Au reconstruction. Inside a unit cell (7×25 nm^2 with the long lattice parameter slightly varying along the sample), two nanoislands are arranged. By increasing the coverage θ_{Co}, the dots grow laterally until they coalesce to form a quasicontinuous thin film at around 1.5 ML.[25] When $\theta_{\mathrm{Co}} = 0.5$ ML the dots are well isolated with a mean diameter $d \simeq 5.5$ nm. A typical STM image of this system is shown in Fig. 1(a).

The Co nanodots were covered with a Pt overlayer in the range $\theta_{\mathrm{Pt}} = 0.5$–$2.5$ ML. Figure 1(b) displays an STM image of the system when half a monolayer of Pt is deposited. The original size and shape distributions of Co nanodots remain almost unchanged, while Pt mainly forms monolayer rims which surround laterally the dots. As deduced from a profile analysis of the STM images [Fig. 1(c)], the height of the rim is around 2.3 Å in accordance with the tabulated 2.26 Å distance between two Pt crystallographic planes along the (111) direction. At this stage the rims of adjacent islands begin to coalesce even if the typical shape is prevalently bulged in the direction perpendicular to the island rows. A complete capping of the nanodots is achieved if the Pt coverage is increased further, but the initial organization in the array still remains visible. Indeed, if $\theta_{\mathrm{Pt}} = 1.5$ ML, Pt forms a quasicontinuous 2 ML thick film while the third layer is mainly on the top of Co dots. Figure 1(d) shows that the growth of Pt proceeds uniformly in a layer-by-layer mode, with the second monolayer being almost complete before the formation of the third one. A similar behavior was observed for Pt/Au(111) heteroepitaxy,[26] so that the Frank-van der Merwe growth of Pt is only partially disturbed by the presence of Co dots. In contrast, on a Co(0001) single crystal, Pt was observed to grow in a Volmer-Weber mode.[27,28]

As pointed out previously,[20] the variations of interatomic distances in the Co core with capping can be a key point for the understanding of the magnetic properties. Direct atomic resolution with STM is inherently limited to uncovered magnetic particles and is not suitable for core-shell systems. Therefore, we studied both by SEXAFS and molecular-dynamics simulations the changes of interatomic distances in Co nanodots before and after Pt capping. For SEXAFS measurements, two samples consisting first of around 0.5 ML of Co/Au(111) and second of the same Co coverage covered with around 3 ML of Pt were prepared *in situ*. The SEXAFS spectra in NI and GI for core-shell Co/Pt nanodots are represented on Fig. 2. A quantitative analysis of the spectra can be obtained using the classical procedure described in Ref. 29. We calculated the Fourier transform of the spectra, and the inverse Fourier transform of its first peak allowed us to isolate the contribution of the first-nearest-neighbor (NN) from the total SEXAFS signal. This contribution was then fitted using

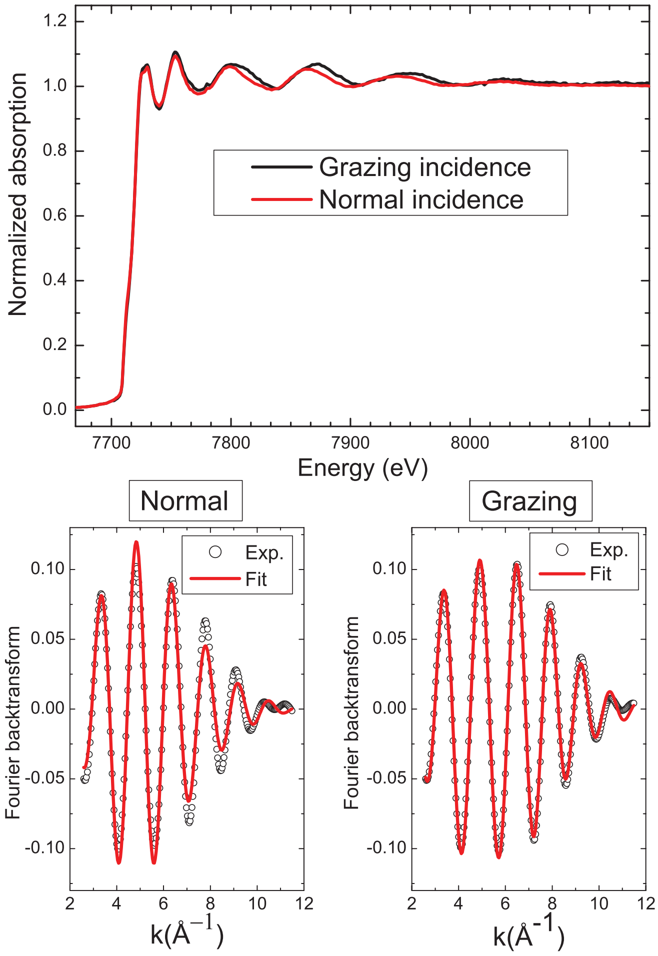

FIG. 2. (Color online) (Top) Raw Co K edges absorption of a 0.5 ML Co covered by 3 ML of Pt in normal and grazing geometry. (Bottom) Fourier backtransforms of the signal (open dots) in the normal (left) and grazing (right) geometry with the fits (red lines) as described in the text.

TABLE I. Effective coordination number N^*, nearest-neighbor distances R and disorder σ^2 for uncapped 0.5 ML Co dots (top part) and 3 ML Pt capped 0.5 ML Co dots (bottom part).

Incidence		N*	R (Å)	σ^2 (1×10^{-3}Å^2)
Grazing	Co-Co⊥	6	2.46	3.4
	Co-Co∥	0		
Normal	Co-Co⊥	1.5	2.46	3.4
	Co-Co∥	9	2.51	12.4
Grazing	Co-Pt⊥	3	2.59	4.0
	Co-Co⊥	6	2.50	9.1
	Co-Co∥	0		
Normal	Co-Pt⊥	0.75	2.59	4.0
	Co-Co⊥	1.5	2.50	9.1
	Co-Co∥	9	2.55	15.6

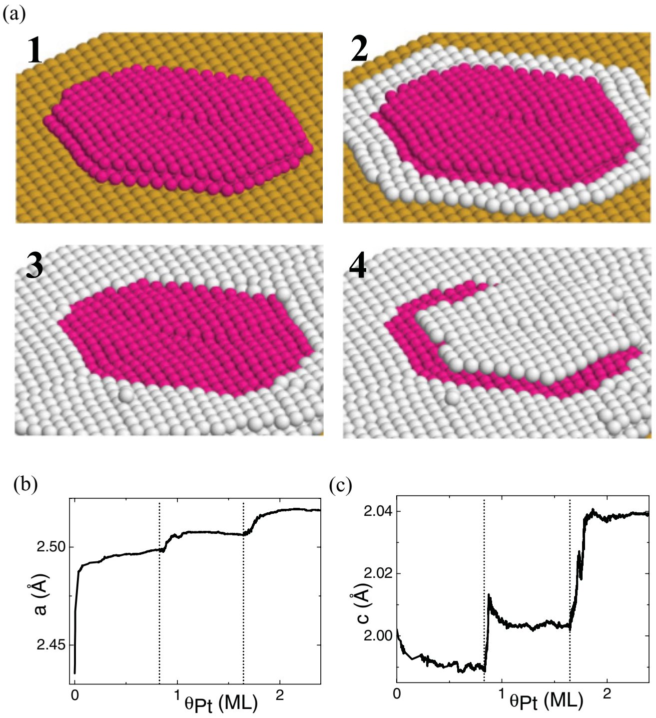

FIG. 3. (Color online) (a) Different sketches of the encapsulation process. 1: Raw 585 Co atoms cluster. 2: Surrounded by 200 Pt atoms ($\theta_{\mathrm{Pt}} = 0.125$ ML). 3: Surrounded by 2000 Pt atoms ($\theta_{\mathrm{Pt}} = 1.25$ ML). 4: Surrounded by 2900 Pt atoms ($\theta_{\mathrm{Pt}} = 1.8$ ML). (b) Change of the mean in-plane Co-Co distance with encapsulation. (c) Change of the distance between Co planes with encapsulation. The vertical dotted lines indicate the completion of the first and second Pt layer around the Co core.

the SEXAFS formula in the single scattering approximation.[29] Amplitude and phase functions for the Co-Co pair were determined from a bulk Co reference spectrum, and for the Co-Pt pair they were calculated from the FEFF software[30] and applied on an experimental $\mathrm{CoPt_3}$ SEXAFS spectrum for confirmation. Due to the polarization dependence of SEXAFS oscillations, the number of NN arising in the fit is an effective coordination number $N^* = \sum_i 3\cos^2\alpha_i$ (where α_i is the angle between the polarization vector of the x ray and the bond i[31,32]). We used the same fitting procedure as in Ref. 33: N^* fixed to theoretical values for large bilayer islands and neglecting the in-plane Pt NN contribution. We also neglected the Au NN contribution as discussed below. For each sample, we have first fitted the GI spectrum to get the out-of-plane NN distance (Co-Co and Co-Pt). It is worth noting that the fitting procedure is not very sensitive to the Pt capping layer and that the Co-Pt NN distance is unprecise. Using these values, we fitted the NI spectrum and deduced the in-plane NN distance (Co-Co). These distances were obtained with an associated Debye-Waller factor σ^2, giving the width of the radial-distribution function of the first NN shell parallel and perpendicular to the interface. The results of the fits are presented in Table I and compared with the experimental data in Fig. 2. It is first interesting to note that a good fit can be obtained by keeping the coordination numbers for Co unchanged after Pt capping, which indicates that under our growth conditions the mixing between the two elements is weak, giving rise to a core-shell geometry. Focusing on the Co core, one observes that for both samples the Co crystallographic structure is anisotropic with an in-plane Co-Co distance larger than the out-of-plane Co-Co distance. Moreover, these distances increase when the dots are covered by Pt. The in-plane NN distance increases from 2.51 Å (the same value as in bulk cobalt) to 2.55 Å, and the out-of-plane Co NN distance increases from 2.46 to 2.50 Å (i.e., the interplane distance varying between 2.01 and 2.04 Å). The capping with Pt also induces an increase of the disorder (σ^2). For both cases, the Co dots are not in coherent epitaxy on the Au substrate, probably due to the large lattice mismatch (14%), and this result justifies the fitting procedure where the Au contribution is neglected.[33] This interfacial disorder can also explain that the fitting procedure is not very sensitive to the topmost Pt layer.

In order to have a more detailed view of the structural changes in the Co dots during Pt encapsulation, we performed complementary molecular-dynamics calculations on this system. As suggested by the STM and SEXAFS data, a tendency to mixing between Co and Pt was avoided in the simulations by a direct quenching of the system. This also allows us to compare the influence of Pt capping with Au capping on the same system.[20] Sketches of the initial Co dot and the progressive encapsulation by Pt are shown in Fig. 3(a). In order to compare with SEXAFS results, we have plotted the variation of the mean in-plane Co-Co distance [averaged over the two Co planes; cf. Fig. 3(b)] and the variation of the distance between the two Co planes [cf. Fig. 3(c)]. Note that the main variation of these parameters occurs after the completion of Pt layers, when Pt rims (or an overlayer) surround the Co island. Concerning the interplane distance, the agreement with SEXAFS is excellent, molecular dynamics indicating a 1.6% increase of the interplane distance from 2.00 Å for raw Co to 2.04 Å for a 2.6 ML Pt capping. The in-plane parameter shows also an increase with the Pt capping by 3.4% with molecular dynamics, as compared to the 1.6% measured by SEXAFS. Looking in more detail, the in-plane parameter of the raw Co cluster is smaller by molecular-dynamics calculations (2.44 Å) as compared to the measured one (2.51 Å). This discrepancy can be ascribed to a size effect and the rough description of the Au surface. Indeed, for the computational time issue, the cluster calculated in molecular dynamics is smaller than the experimental ones and the Au surface is unreconstructed. As shown previously,[17] taking into account such refinements gives an in-plane value closer to the experimental data.

The global behavior of platinum encapsulation is very similar to the gold one.[20] The main difference lies in the amplitude of the strain. Moreover, in the case of the mean Co-Co in-plane distance, the stronger expansion is at the completion of the second gold layer while it is at the first one for platinum. This certainly results from both the stronger Pt-Co interaction than Au-Co and the different chemical nature of the encapsulating metal with respect to the substrate.

B. Magnetic properties of Co/Pt nanodots

The magnetic properties and more particularly the change of magnetic anisotropy with Pt capping were studied by both XMCD and MOKE techniques. We have first measured the magnetic moment of Co in both uncovered and Pt covered configurations on two different samples realized in identical experimental *in situ* conditions with a Co coverage around 0.4 ML and a Pt overlayer around 2.5 ML. XMCD spectra across the Co $L_{2,3}$ edges [cf. Fig. 4(a)] permitted us to obtain the orbital μ_L and spin magnetic moments μ_S, from angle-resolved measurements and by using magneto-optical sum rules.[34] The number of holes in the 3d band was taken as 2.49.[35] From our measurements the effect of Pt capping was to increase slightly μ_S, which rises from 1.65 ± 0.05 to 1.75 ± 0.05 μ_B/atom. The orbital magnetic moment per atom was also observed to increase, since μ_L rises from 0.18 ± 0.03 to 0.24 ± 0.03 μ_B/atom. Magnetization cycles were obtained by recording the intensity variation of the XMCD signal at the L_3 edge as a function of the applied magnetic field and sample temperature. A complete magnetization loop was taken in 110 s. The results obtained for the Co dots covered with Pt are reported in Fig. 4(b). If the cycles were measured along the surface normal direction ($\alpha = 0^\circ$) at temperatures lower than 50 K, the intensity of the field was not sufficient to saturate the sample magnetization and minor loops were observed. At higher temperatures, saturation was reached and the coercive field (which at $T = 50$ K was around 2.5 T) decreased gradually and vanished around 150 K, indicating the transition between blocked macrospin and superparamagnetism. The square shape of the loops at $\alpha = 0^\circ$ demonstrates that the easy axis lies out of plane, as is more evident from the comparison with the loops taken at $\alpha = 60^\circ$. In this latter case the loops assumed a sigmoidal shape and saturation was never achieved with the maximum field intensity. Such an angular dependence is in agreement with the prediction of the Stoner-Wohlfarth model,[36] confirming that the hard axis lies in the sample plane. The experimental hysteresis loops were fitted with a model previously reported[37] and extended to $\alpha \neq 0^\circ$. Briefly, the nanoparticles are regarded as a two-level system (the Ising model) and its dynamics is described in the framework of the transition state theory. The magnetization reversal is derived from the rate law, and the switching rates are expressed with Arrhenius equations. The small polydispersity of the dots is taken into account by assuming a Gaussian distribution of MAE. For the Pt covered sample, the best fits, taking a mean value for $\mu_{\text{tot}} = 1.8$ μ_B, were obtained for islands containing $N = 760$ atoms each, with a mean magnetic anisotropy $\bar{K} = 0.36$ meV/atom and a standard deviation $\sigma_K = 0.09$ meV/atom. The same procedure was performed on Co nanoislands without the Pt overlayer. In this case we obtained, for $\mu_{\text{tot}} = 1.7$ μ_B, $N = 780$ atoms, $\bar{K} = 0.29$ meV/atom, and $\sigma_K = 0.11$ meV/atom. From these

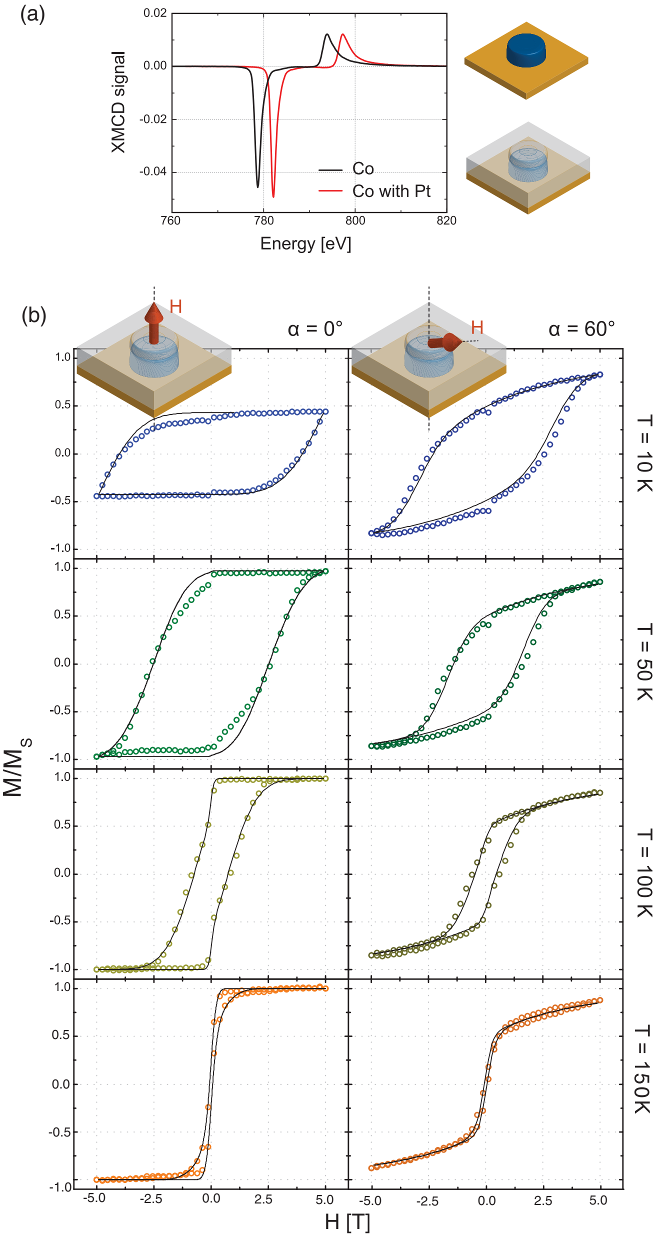

FIG. 4. (Color online) (a) Normalized XMCD signal at the L_3 and L_2 Co edges recorded on the 0.4 ML Co/Au(111) (black curve) and on the 2.5 ML Pt on 0.4 ML Co/Au(111) (gray curve, red online, shifted by 3 eV for clarity). (b) Experimental magnetization curves determined with XAS at the L_3 Co edge (open circles) for Pt (2.5 ML)/Co (0.4 ML)/Au(111) at different temperatures T and angles α. The zero-field anomaly is due to a reproducible experimental overdetection in the sample electron current at zero field. The full lines represent the best fit according to the model described in the text.

results we obtained that the mean activation energy for magnetization reversal $\bar{E}_{\rm a}$ rises from 226 to 274 meV, i.e., a 21% increase with Pt capping.

The change in the MAE with Pt capping could be investigated step by step with MOKE by studying the magnetic susceptibility as a function of the temperature. Concretely, the measurements were performed before and just after the deposition of Pt, from the submonolayer to the full capping regime. Every Pt coverage corresponded to a new sample with the Pt growth done in a single shot. The initial self-organized Co nanodots corresponded to a 0.4 ML coverage, i.e., as close as possible to the XMCD samples, taking into account that the XMCD and MOKE experiments were realized in different UHV setups. Typical results are reported in Fig. 5(a). In all the cases, the susceptibility χ' reveals a transition between a blocked and a superparamagnetic regime, as expected for single domain nanodots. The transition between these two regimes takes place at different blocking temperatures, depending on $\theta_{\rm Pt}$. The blocking temperature $T_{\rm B}$ is directly proportional to the activation energy for magnetization reversal $E_{\rm a}$: $T_{\rm B} = E_{\rm a}/k_{\rm B}\ln(\nu_0/\omega)$, where ν_0 is the attempt frequency for reversal and ω is the angular frequency of the applied magnetic field. According to the macrospin model, $E_{\rm a} = N.K$ where N is the number of magnetic atoms inside the dot and K is the mean magnetic anisotropy per atom. It is worth noting that this latter assumption is not perfectly exact and can be applied only for the very small Co dot sizes considered in this work.[13] To understand how the activation energy changes upon Pt covering, the experimental data were fitted with a model in which the dynamical susceptibility is expressed according to the linear-response theory of a uniaxial system. Among all the possible orientations, the magnetization can lie only along the easy axis (for this reason it is also called the Ising model). In this case we obtain the simple analytical expression

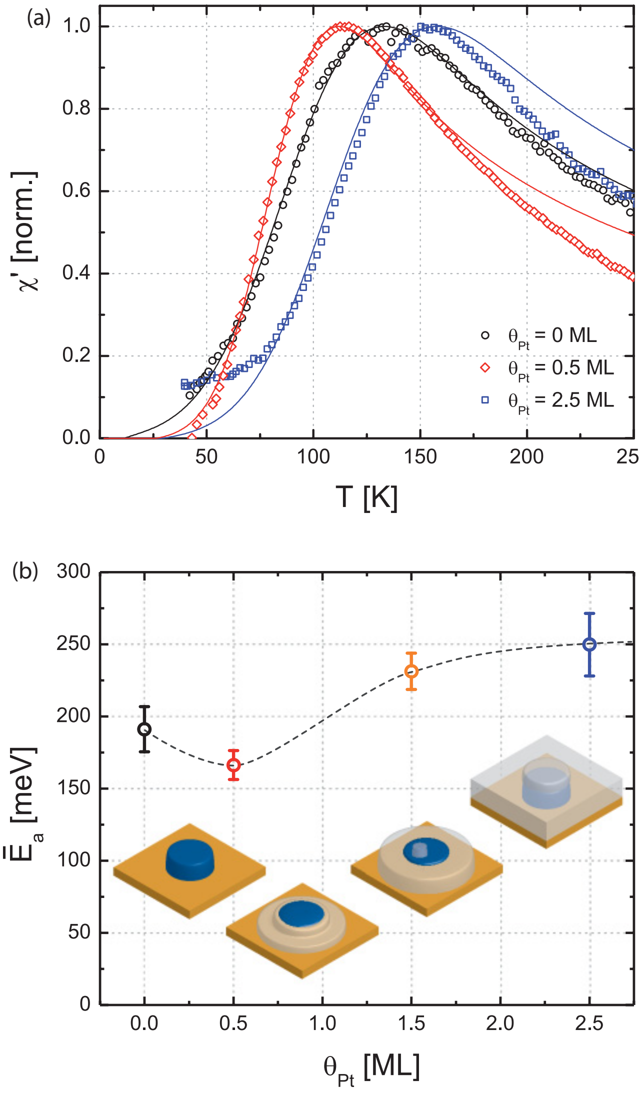

FIG. 5. (Color online) (a) Change in the temperature dependence of the magnetic susceptibility of Co nanodots (black circles) upon Pt capping (colored diamonds); the coverage of the Pt overlayer is reported in the legend. The experimental data (open symbols) were fitted with the model described in the text (continuous line). (b) Mean activation energy for magnetization reversal as a function of Pt coverage as deduced from Eq. (2). The statistical dispersion around mean values is $\sigma_E \simeq 0.25\,\bar{E}_{\rm a}$. All the measurements have been repeated with a good reproducibility, the standard deviations being the error bars. The dashed line is drawn as a guide for the eye. In the inset, a schematic representation of the system is reported for each $\theta_{\rm Pt}$ studied.

$$\chi'_{\rm dot} = \frac{N^2\mu_{\rm at}^2}{k_{\rm B}T}\,\frac{1}{1+\omega^2\left(e^{E_{\rm a}/k_{\rm B}T}/\nu_0\right)^2}, \qquad (1)$$

where we have taken $\mu_{\rm at} = 1.8\ \mu_{\rm B}$/atom, the magnetic moment per atom, as a mean value of XMCD measurements, $\omega = 2\pi f$, $f = 1$ Hz is the frequency of the applied alternating magnetic field, and $\nu_0 = 40$ GHz is the attempt frequency for magnetization reversal.[13] Since we are considering a large ensemble of nanodots, their activation energy also follows a certain distribution, reflecting their magnetic anisotropy distribution. This latter is assumed to be Gaussian, with mean $\bar{E}_{\rm a}$ and standard deviation σ_E. Thus, the total susceptibility takes the expression

$$\chi' = \sum_{E_{\rm a}} \chi'_{\rm dot}\,\frac{e^{\frac{(E_{\rm a}-\bar{E}_{\rm a})^2}{2\sigma_E^2}}}{\sqrt{2\pi}\,\sigma_E}\,\delta E_{\rm a}. \qquad (2)$$

The best-fit results for the activation energy as a function of Pt coverage are reported in Fig. 5(b). As can be seen, $\bar{E}_{\rm a}$ decreases (around 15%) upon the deposition of a Pt overlayer of submonolayer thickness, which causes the formation of metal rims around Co nanodots. In contrast, when Co nanodots are completely encapsulated (2.5 ML Pt coverage) $\bar{E}_{\rm a}$ is increased up to 35% in good agreement with XMCD results.

III. ANALYSIS AND DISCUSSION

A. Influence of interfacial mixing

Until now, an important point has been disregarded. Co and Pt are miscible metals and *a priori* one could expect the formation of a Co-Pt alloy at the interface between the core and shell of the nanodots. Indeed, this phenomenon was already observed for Pt/Co core-shell clusters.[38,39] On the other hand, as pointed out in Sec. II A, SEXAFS measurements did not

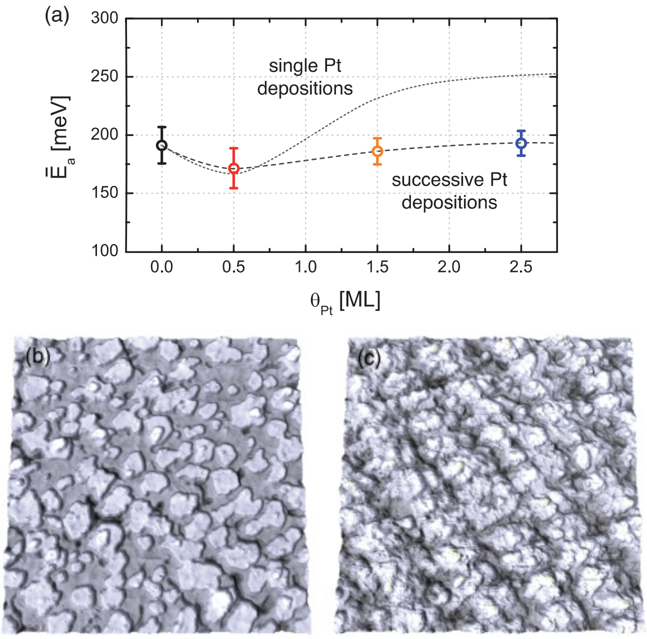

FIG. 6. (Color online) (a) Mean activation energy for magnetization reversal of Co nanodots as a function of θ_{Pt}, if the overlayer is deposited in successive steps. As a comparison, the results for the single steps case [as in Fig. 5(b)] are also reported in dotted lines. (b) STM images (80 × 80 nm^2) showing the different morphology of a 2.5 ML thick Pt overlayer when deposited in single (left) or in successive steps (right).

show any evidence of interdiffusion. We can thus conclude that the achievement of a sharp Co/Pt interface is due to the growth kinetics of the Pt layer, which is fast enough to avoid alloy formation. When the deposition of the overlayer was slower, MOKE experiments showed remarkable differences, which we attribute to interface mixing. This is shown in Fig. 6(a), where the activation energy for magnetization reversal is reported as a function of θ_{Pt}, if the Pt layer is deposited at the same flux rate but in successive steps. The trend is qualitatively the same if Pt is deposited in a single shot (Sec. II B), but with a strong reduction of the effect. We conclude that the system has enough time (few days) to evolve toward thermodynamical equilibrium and partially mixes. In $\mathrm{Co}_x\mathrm{Pt}_{1-x}$ supported nanodots, the MAE per Co atoms is lower than in pure Co nanodots since in this disordered alloy Pt essentially reduces the out-of-plane anisotropy.[40] Thus, the intermixing limits the increasing of $\bar{E}_{\mathrm{a}}$ observed in the case of a sharp Co/Pt interface. This hypothesis is supported by the STM study of the surface morphology. As shown in Fig. 6(b), if a single deposition is performed, the growth proceeds clearly with a layer-by-layer mode, while in the successive deposition case, as shown in Fig. 6(c), the Pt layer shows high roughness and protrusions, which are symptomatic of a nonperfect crystalline atomic arrangement. Interface alloying could explain this finding since it causes disorder in the atomic arrangement and disturbs further atoms packing in the surroundings. To summarize, STM and MOKE measurements gave us significant evidence of the importance of kinetics in Co/Pt core-shell nanodots. If the sample has enough time to evolve (typically one day in our case), we observed a rough morphology of the Pt overlayer and a reduction of the change in Co magnetic properties. Both these effects can be ascribed to interface alloying, which naturally occurs due to the Co and Pt miscibility.

B. Origin of magnetic anisotropy in Co/Pt core-shell nanodots

Our magnetic measurements indicate that the Co nanodots maintain their individual superparamagnetic behavior upon Pt capping. Indeed, the amplitude of the measured susceptibility does not decrease with capping, as would be expected for interacting particles.[41] Generally, one could expect the rising of Ruderman-Kittel-Kasuya-Yosida (RKKY) interactions between a dot and the surrounding ones. Signatures of this indirect exchange through Pt atoms were observed in Co/Pt multilayers,[42] in spin-glass behavior of three-dimensional Co nanoparticles embedded in a Pt matrix,[43] and more recently in Co adatoms on Pt(111).[44] However RKKY interaction changes its sign on the atomic scale, and thus, in our case, this effect seems to be smeared out over neighboring circular 5 nm dots.[45] Since we rule out the occurrence of significant interparticle interactions, the change of Co blocking temperature must be due to a modification of MAE inside each single dot.

This brings us to the central issue of the discussion, the identification of physical phenomena which modify Co magnetism. To this scope, it is useful to compare the present results with previously reported ones, in which Co nanodots were covered with an Au overlayer.[20] In this case, equivalent MOKE measurements showed that Au capping causes a change in the activation energy which is opposite to the one induced by Pt capping. Indeed, $\bar{E}_{\mathrm{a}}$ was observed to increase initially with submonolayer Au coverage and then decrease in the full capping regime. This magnetic behavior was explained by assuming a dominant role of magnetoelasticity, using tabulated magnetoelastic constants for Co.[46] Indeed, an Au metallic rim induced an in-plane strain which caused an increase of MAE, while if the islands were completely covered an additional vertical dilatation occurred and the overall effect was an MAE decreasing. As indicated by SEXAFS measurements and molecular-dynamics simulations, the elastic effect on Co islands is qualitatively the same for Pt but with smaller dilatations.[20] The magnetoelastic contribution of the Co core should therefore be qualitatively similar, although smaller in amplitude, to the one reported with Au capping. This trend is in disagreement with our XMCD and MOKE experiments [cf. Fig. 5(b)].

In order to discuss these opposite trends, we now analyze the differences between the two metals. Unlike Au, Pt has an important density of states close to the Fermi level. This implies a larger overlap with the 3*d* Co density of states and a larger hybridization between the two metals. As a further consequence, Pt nearly satisfies the Stoner criterion and gets easily polarized by neighboring magnetic atoms. The difference between the two metals when interfaced with Co is highlighted in a theoretical work in which the magnetic moments of small Co clusters on Au(111) and Pt(111) were calculated.[47] In Pt, significant induced spin and orbital moments are observed, while the polarization effect is negligible for Au. The different behavior of the two metals was confirmed experimentally in the case of thin films. XMCD measurements have shown that the total magnetic momentum induced in Au atoms is around one order of magnitude smaller than in Pt. Indeed, at the Au/Co interface $\mu_{\mathrm{Au}} = 0.031\ \mu_{\mathrm{B}}/\mathrm{atom}$.[48] On the other hand, in a Pt/Co bilayer Pt atoms acquire a magnetic momentum of $\mu_{\mathrm{Pt}} = 0.61\ \mu_{\mathrm{B}}/\mathrm{atom}$ and the magnetic polarization exponentially decays with the distance from Co.[49] Moreover, in the case of Co/Pt multilayers it has been proposed that it is the interfacial hybridization between Co and Pt that produces an enhancement of MAE.[50]

Based on all these observations we can propose the following interpretation. When Co nanodots are covered with Au, band hybridization can be neglected and the magnetic anisotropy is modified mainly by the magnetoelasticity of the Co core.[20] In the case of Pt capping, band hybridizations are more pronounced, favoring the alignment of local spins with the Co-Pt bonds. In this case, a submonolayer Pt capping of Co nanodots increases the number of in-plane Co-Pt bonds, decreasing the initial out-of-plane MAE. In contrast, the capping of the top Co layer induces out-of-plane Co-Pt bonds and therefore increases the out-of-plane MAE, as observed experimentally. This origin of MAE by hybridization seems to be dominant over the small magnetoelastic component.

It is also worth noting that our observations on nanometer scale clusters are different from ultrathin films. By studying how the metal overlayer influences the spin reorientation transition of Co thin films, Pt and Au capping were observed to behave qualitatively in the same way,[8,51] i.e., an increase of the out-of-plane magnetic anisotropy. The dominant effect was identified to be an interface anisotropy, generally ascribed to band hybridizations. However, few experimental and theoretical works have pointed out that the Co/Au interface anisotropy could be dominated by magnetoelastic effects.[52–54] In contrast, different theoretical works on FePt and CoPt alloys have pointed out the crucial importance of electronic hybridizations and correlations in their large magnetocrystalline anisotropy.[55,56] We therefore believe that the microscopic origin of magnetic anisotropy is similar in ultrathin films as compared to nanodots but that the strain variations with capping are very different due to a change of dimensionality (from two- to zero-dimensional). Realistic *ab initio* calculations on such systems, considering the complexity of nonpseudomorphic interfaces, could certainly confirm in the future the different microscopic origins of magnetic anisotropy in Co/Au and Co/Pt systems.

IV. CONCLUSIONS

In the present paper, we have studied the growth and magnetism of Co/Pt core-shell nanodots. Pt was deposited as an overlayer on self-organized Co nanodots on Au(111). Structural and magnetic measurements were coupled in order to identify the main phenomena acting at the Co/Pt interface. In a submonolayer regime, Pt forms metal rims around Co nanodots, and the Co magnetic anisotropy decreases. On the other hand, if more than one monolayer of Pt is deposited, the Co dots are completely covered and their magnetic anisotropy is enhanced. This MAE change is exactly the opposite trend that was observed with a Au capping, whereas the strain inside the Co core when capped with Pt and Au behaves qualitatively the same (in-plane and out-of-plane dilatations). To interpret our experimental observations, we have identified three main phenomena at the Co/Pt interface: intermixing, magnetoelasticity, and band hybridization. Our results indicate that the main one is band hybridization, which is responsible for the observed increase of magnetic anisotropy with full Pt capping. Intermixing and magnetoelasticity have rather the opposite effect and tend to decrease the MAE. To understand the interplay between these different phenomena is fundamental in order to tune the magnetic properties of nanoparticles for precise applications, from data storage to biomedical research, and should help global MAE engineering in nanostructures.

ACKNOWLEDGMENTS

We acknowledge the European Synchrotron Radiation Facility and SOLEIL for provision of synchrotron radiation facilities. We acknowledge expert assistance of the ID08 staff at ESRF and of the SAMBA staff at SOLEIL for beamline settings. The authors thank A. Sassella for fruitful discussions. We acknowledge financial support from ANR ETNAA. V. R. thanks Institut Universitaire de France for support.

---

[*] Also at Department of Materials Science, Universitá degli Studi di Milano-Bicocca, Via R. Cozzi 53 Milano IT-20125, Italy.

[†] vincent.repain@univ-paris-diderot.fr.

[1] A. Lu, E. Salabas, and F. Schüth, Angew. Chem. Int. Ed. **46**, 1222 (2007).

[2] J. Gao, H. Gu, and B. Xu, Acc. Chem. Res. **42**, 1097 (2009).

[3] M. Johnson, P. Bloemen, F. Broeder, and J. Vries, Rep. Prog. Phys. **59**, 1409 (1996).

[4] N. Weiss *et al.*, Phys. Rev. Lett. **95**, 157204 (2005).

[5] D. Weller and A. Moser, IEEE Trans. Magn. **35**, 4423 (1999).

[6] S. Rusponi, T. Cren, N. Weiss, M. Epple, P. Buluschek, L. Claude, and H. Brune, Nat. Mat. **2**, 546 (2003).

[7] P. Gambardella *et al.*, Science **300**, 1130 (2003).

[8] C. Train, R. Megy, and C. Chappert, J. Magn. Magn. Mater. **202**, 321 (1999).

[9] P. F. Carcia, J. Appl. Phys. **63**, 5066 (1988).

[10] D. Weller, Y. Wu, J. Stöhr, M. Samant, B. Hermsmeier, and C. Chappert, Phys. Rev. B **49**, 12888 (1994).

[11] B. Voigtländer, G. Meyer, and N. Amer, Phys. Rev. B **44**, 10354 (1991).

[12] H. Dürr, S. Dhesi, E. Dudzik, D. Knabben, G. V. Laan, J. Goedkoop, and F. Hillebrecht, Phys. Rev. B **59**, R701 (1999).

[13] S. Rohart, P. Campiglio, V. Repain, Y. Nahas, C. Chacon, Y. Girard, J. Lagoute, A. Thiaville, and S. Rousset, Phys. Rev. Lett. **104**, 137202 (2010).

[14] V. Briois, E. Fonda, S. Belin, L. Barthe, C. L. Fontaine, F. Langlois, M. Ribbens, and F. Villain, UVX 2010, 41 (2011).

[15] V. Rosato, M. Guillopé, and B. Legrand, Philos. Mag. A **59**, 321 (1989).

[16] C. Goyhenex and H. Bulou, Phys. Rev. B **63**, 235404 (2001).

[17] I. Chado, C. Goyhenex, H. Bulou, and J. P. Bucher, Phys. Rev. B **69**, 085413 (2004).

[18] L. Verlet, Phys. Rev. **159**, 98 (1967).

[19] W. C. Swope, H. C. Andersen, P. H. Berens, and K. R. Wilson, J. Chem. Phys. **76**, 637 (1982).

[20] Y. Nahas, V. Repain, C. Chacon, Y. Girard, J. Lagoute, G. Rodary, J. Klein, S. Rousset, H. Bulou, and C. Goyhenex, Phys. Rev. Lett. **103**, 067202 (2009).

[21] J. Stöhr, J. Magn. Magn. Mater. **200**, 470 (1999).

[22] J. Barth, H. Brune, G. Ertl, and R. Behm, Phys. Rev. B **42**, 9307 (1990).

[23] V. Repain, G. Baudot, H. Ellmer, and S. Rousset, Europhys. Lett. **58**, 730 (2002).

[24] C. Tölkes, P. Zeppenfeld, M. Krzyzowski, R. David, and G. Comsa, Phys. Rev. B **55**, 13932 (1997).

[25] S. Padovani, I. Chado, F. Scheurer, and J. Bucher, Phys. Rev. B **59**, 71815 (1999).

[26] M. Pedersen, S. Helveg, A. Ruban, I. Stensgaard, E. Lægsgaard, J. Nørskov, and F. Besenbacher, Surf. Sci. **426**, 395 (1999).

[27] H. Bulou, A. Barbier, R. Belkhou, C. Guillot, B. Carrière, and J. Deville, Surf. Sci. **352–354**, 828 (1996).

[28] G. Cabeza, P. Légaré, A. Sadki, and N. Castellani, Surf. Sci. **457**, 121 (2000).

[29] D. Sayers, E. Stern, and F. Little, Phys. Lett. **27**, 1204 (1971).

[30] S. I. Zabinsky, J. J. Rehr, A. Ankudinov, R. C. Albers, and M. J. Eller, Phys. Rev. B **52**, 2995 (1995).

[31] P. Roubin, D. Chandesris, G. Rossi, J. Lecante, M. Desjonquères, and G. Tréglia, Phys. Rev. Lett. **56**, 1272 (1986).

[32] O. Heckmann, H. Magnan, P. Le Fèvre, D. Chandesris, and J. Rehr, Surf. Sci. **312**, 62 (1994).

[33] N. Marsot, R. Belkhou, H. Magnan, P. Le Fèvre, C. Guillot, and D. Chandesris, Phys. Rev. B **59**, 3135 (1999).

[34] P. Carra, B. Thole, M. Altarelli, and X. Wang, Phys. Rev. Lett. **70**, 694 (1993).

[35] C. Chen, Y. Idzerda, H. Lin, N. Smith, G. Meigs, E. Chaban, G. Ho, E. Pellegrin, and F. Sette, Phys. Rev. Lett. **75**, 152 (1995).

[36] E. Stoner and E. Wohlfarth, Philos. Trans. R. Soc. London A **240**, 599 (1948).

[37] S. Rohart, V. Repain, A. Tejeda, P. Ohresser, F. Scheurer, P. Bencok, J. Ferré, and S. Rousset, Phys. Rev. B **73**, 165412 (2006).

[38] M. Négrier, J. Tuaillon-Combes, V. Dupuis, P. Mélinon, A. Perez, and A. Traverse, Philos. Mag. A **81**, 2855 (2001).

[39] J. Arbiol, F. Peiró, A. Cornet, C. Clavero, A. Cebollada, G. Armelles, and Y. Huttel, Appl. Phys. Lett. **86**, 032150 (2005).

[40] N. Moreau, V. Repain, C. Chacon, Y. Girard, J. Lagoute, S. Rousset, F. Scheurer, and P. Ohresser (unpublished).

[41] J. Andersson, C. Djurberg, T. Jonsson, P. Svedlindh, and P. Norblad, Phys. Rev. B **56**, 13983 (1997).

[42] J. Knepper and F. Yang, Phys. Rev. B **71**, 224403 (2005).

[43] J. Bartolomé, L. García, F. Bartolomé, F. Luis, F. Petroff, C. Deranlot, F. Wilhelm, and A. Rogalev, J. Magn. Magn. Mater. **317**, e9 (2007).

[44] F. Meier, L. Zhou, J. Wiebe, and R. Wiesendanger, Science **320**, 82 (2008).

[45] R. Skomski, Europhys. Lett. **48**, 455 (1999).

[46] D. Sander, Rep. Prog. Phys. **62**, 809 (1999).

[47] O. Sipr, S. Bornemann, J. Minár, S. Polesya, V. Popescu, A. Simnek, and H. Ebert, J. Phys. Condens. Matter **19**, 096203 (2007).

[48] F. Wilhelm, M. Angelakeris, N. Jaouen, P. Poulopoulos, E. Papaioannou, C. Mueller, P. Fumagalli, A. Rogalev, and N. Flevaris, Phys. Rev. B **69**, 220404 (2004).

[49] M. Suzuki, H. Muraoka, Y. Inaba, H. Miyagawa, N. Kawamura, T. Shimatsu, H. Maruyama, N. Ishimatsu, Y. Isohama, and Y. Sonobe, Phys. Rev. B **72**, 054430 (2005).

[50] N. Nakajima, T. Koide, T. Shidara, H. Miyauchi, H. Fukutani, A. Fujimori, K. Iio, T. Katayama, M. Nývlt, and Y. Suzuki, Phys. Rev. Lett. **81**, 5229 (1998).

[51] P. Beauvillain, A. Bounouh, C. Chappert, R. Mégy, S. Ould-Mahfoud, J. Renard, P. Veillet, D. Weller, and J. Corno, J. Appl. Phys. **76**, 6078 (1994).

[52] A. Murayama, K. Hyomi, J. Eickmann, and C. M. Falco, Phys. Rev. B **60**, 15245 (1999).

[53] S. Padovani, F. Scheurer, I. Chado, and J. P. Bucher, Phys. Rev. B **61**, 72 (2000).

[54] C. Chappert and P. Bruno, J. Appl. Phys. **64**, 5736 (1988).

[55] S. Ostanin, S. S. A. Razee, J. B. Staunton, B. Ginatempo, and E. Bruno, J. Appl. Phys. **93**, 453 (2003).

[56] A. B. Shick and O. N. Mryasov, Phys. Rev. B **67**, 172407 (2003).